ANALYSIS OF THE EFFECTS OF 3DP PARAMETERS ON PART FEATURE DIMENSIONAL ACCURACY

Tamas D. Szucs and Dermot Brabazon
School of Mechanical and Manufacturing Engineering, Dublin City University, Ireland

Abstract

3D printing (3DP) is a widely investigated scaffold manufacturing process for Tissue Engineering (TE). Useful scaffold geometries should have high porosity (60-80%) with small (100-500 μm) interconnected pores. Therefore dimensional accuracy on the micron level is one of the crucial parameters of the bone scaffolds. Previously it was shown that the behavior of scaffold geometries can be well simulated with Finite Element Modeling (FEM) however the prediction of actual strength and stiffness values are dependent on dimensional accuracy. This accuracy is in turn dependent on several parameters including particle size and shape, powder-binder interaction, and machine setup. In this work different scaffold strut sizes (0.3 - 0.5 mm) have been fabricated using two different plaster powders (zp102 and zp130) with variations in shell saturation levels, part print position, and part print orientation. The parameters for each powder were analyzed using a full 3^5 factorial experimental design. It was found that the part size and orientation had a significant effect on the dimensional accuracy while the influence of the shell saturation and position was relatively small. The results allow for better dimensional specification for scaffold geometry fabrication by defining the process parameters in 3DP that may be used further in scaffold accuracy optimization.

Introduction

Tissue engineering aims to produce artificial biological substitutes by using suitable cells in combination with various materials and engineering solutions. This goal is important due to the increasing donor shortage and the potential to improve patient response with tailored and definable scaffold properties [1]. A main approach in tissue engineering is to use the patient's own cells to build up an implant that can augment or replace a tissue function including a complete organ. The fundamental problem is that the cells can proliferate into larger colonies; however they are incapable of forming three-dimensional tissues/organs in vitro [2]. To form a three-dimensional organized tissue the cells need complex mechanical, chemical, and electrical signals which are present in their natural environment [3]. For this reason it is necessary to use a porous matrix called a scaffold to which the cells can attach, proliferate and differentiate in vitro and afterwards this can be inserted to the anatomical defect (Figure 1). This matrix is only necessary until the cells form the desired anatomical shape and gain sufficient mechanical properties to withstand the physiological loading. Therefore scaffolds are ideally made from bioresorbable materials [4].

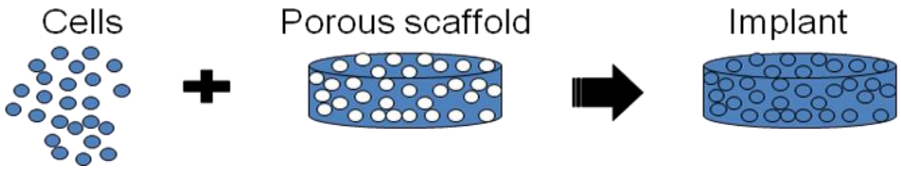

Figure 1 Scaffold use for cell proliferation to produce a functional bio-implant.

In the past few years the number of investigations regarding to Solid Freeform Fabrication (SFF) techniques in manufacturing scaffolds for TE proposes have been significantly increased [5-7]. It is easy to see why this is the case as there is great potential for SFF techniques to manufacture customized products with complex internal geometries. Scaffolds need to incorporate several characteristics that are often contradictory but using FEA combined with SFF can lead to an implant that has been tailored for actual defect properties in the patient.

Due to its complex role the scaffold needs to fulfill requirements in many aspects. Appropriate micro and macro **geometry** including high porosity (50-80%) is required to enhance mass transport which aids nutrient and metabolic waste transport to and from the cells [8]. Moreover the pore structure has to be interconnected to promote tissue integration and vascularisation [9]. The macro geometry of the scaffold has to fit into the complex three-dimensional anatomic defect. To satisfy this requirement medical imaging technologies like Computed Tomography (CT), μCT or Magnetic Resonance Imaging (MRI) can be used for mapping the defect site [10]. Scaffolds should also possess sufficient **mechanical properties** that provide structural support for the cells until the native tissue builds up [2]. The scaffold is ideally made of bioresorbable **material**, with appropriate degradation profile that will dissolve in the body without toxic by-products, thus providing space for new tissue formation. Furthermore appropriate surface chemistry is of high importance in ensuring cell attachment, differentiation and proliferation [11]. Proceeding the SFF period numerous conventional techniques including solvent casting particulate leaching, fiber bonding, membrane lamination, and gas foaming were invented to fabricate porous structures. For example, in solvent casting/particulate leaching, pores are formed by evaporative solvent and pore-forming agent particles that are mixed and cast into a mould and leached out afterwards. This method just like other conventional techniques is incapable of precisely controlling pore size, geometry and spatial distribution. With these techniques, the internal architecture cannot be accurately designed in advance. Moreover there may be no guarantee of the required pore interconnectivity [2]. Using conventional techniques the size of the scaffold can be limited due to difficulties in removal of the porogens. Another important disadvantage is that some these techniques are applying organic solvents during the process that may remain in the scaffold afterwards. These are unfavorable in medical applications due to their carcinogenicity and toxicity. These techniques are also labor demanding, not repeatable and often do not control well the micro and macro geometry of the scaffold. Most of the above listed problems could be overcome by using SFF techniques [6].

Probably the most significant advantage of SFF techniques over the so called conventional scaffold manufacturing techniques is that they can produce more intricate, previously designed and analyzed geometries. Taking advantage of the possibilities of SFF we can have strict control on the porous architecture size, shape and interconnectivity. 3D printing (3DP) is one prospective SFF technique that may be used in manufacturing hard tissues. Currently 3DP is successfully used in various applications including rapid tooling and appearance modeling. However in these cases requirements are often less complex and there are several specific barriers that need to be overcome for hard tissue engineering. In order to design bone substitutes with unique, tailored mechanical properties preliminary FEA is essential. Previous studies have shown that it is possible to characterize the mechanical properties of the structure by changing the pore structure only and keeping the porosity on the same level [12]. Furthermore, it was shown that actual geometry solutions provided from FEA cannot fully be examined experimentally due to dimensional differences between the FEA geometry and that which can be produced from the actual SFF technique [12]. In this work process parameters including powder type, shell saturation, part position, and orientation were examined with the 3D printing

technique. This was done in order to assess the potential for this technology to meet the small scale geometric requirements of hard tissue bone scaffold structures. The results may be interpreted for later studies with biodegradable raw materials.

Materials and methods

Figure 2 presents the specimen geometry that was fabricated in this work. The CAD file dimensions for the cross members were 300 x 300, 400 x 400 and 500 x 500 micrometers and 5 mm in length. Three beams with these dimensions were printed in each test sample. Screening experiments were performed by printing 0.1 to 1.2 mm square cross section beams. Printed beam cross sections of 200 x 200 micrometer and less were not stable enough after printing to support themselves. The minimum beam cross section of 300 x 300 was therefore chosen for this work. The beam sizes chosen are also typical of scaffold beam sizes used in tissue engineering. The geometries for the accuracy measurements were designed using the SolidWorks CAD (SolidWorks Inc., Concorde, MA, USA) program. A ZPrinter 310 (Z Corporation, Burlington, MA) was used to produce the 3DP structures.

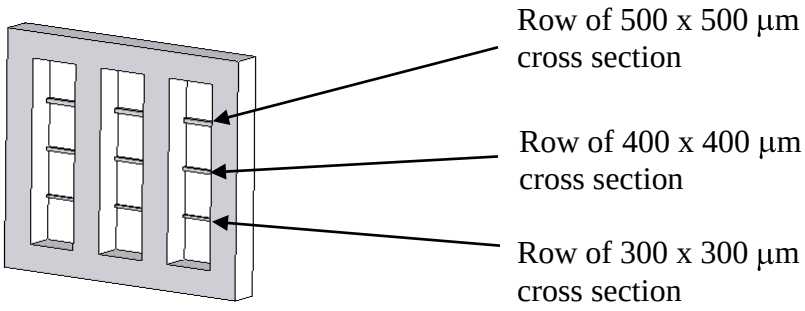

Figure 2 Schematic of the fabricated test frame geometry.

Five different process parameters were investigated. These included location in the x and y axis on the 3DP build bed, the orientation with respect to the machine orthogonal axis, the saturation level, and the beam size (300, 400 and 500 micrometer). Three levels of each of these five parameters were chosen and used in a full factorial design of experiments.

Table 1 summarizes the studied factors and the levels of these factors. For each powder, this resulted in 243 printed test frames fabricated with the associated process parameter combinations. An average value and confidence interval of the beams of similar size were calculated and recorded for each frame structure. In every case the specimens were printed with 0.0875mm layer thickness, bleed compensation set to off and they were left to dry for 24 hours before depowdering. Further description of the factors is presented below.

Levels	**Shell saturation**			**Size**	**Orientation**	**X position**	**Y position**
	Saturation level	Actual binder/volume ratio					
		zp 102	zp 130				
Level 1	75%	0.281747	0.172178	0.3 mm	X	Left	Left
Level 2	100%	0.229571	0.375662	0.4 mm	Y	Center	Center
Level 3	125%	0.469578	0.286964	0.5 mm	Z	Right	Right

Table 1 Factors and levels in the design space for the zp102 and zp130 powders.

Powder type

Two different plaster powders were used, the well known zp102 and the relatively new zp130 with the appropriate binders zb56 and zb58 respectively. According to the manufacturer's specification the zp130 provides improved feature definition that has been investigated in this work. The main difference in processing the two powders is that zp102 powder needs more time to reach its full strength since higher saturation levels are used for this powder both in the shell and the core. The printing speed is higher for the zp130 powder for the same reason. New batches of powder were used for this work and the particle size distributions were analyzed before being used for both powders using the Malvern Mastersizer S (Malvern Ltd., Malvern, UK) particle analyzer.

Shell saturation level

The saturation level determines the depth of binder penetration within the powder [13]. In general increasing the saturation level results in higher strength while lower saturation levels makes depowdering easier. Saturation levels can be set selectively for the shell and core of the part. The default level is noted as 100% for both the shell and the core however the actual saturation is noted as binder volume ratio. This ratio indicates that on default settings the printer head uses higher saturation on the shell. The recommended saturation settings vary with the powder type. In this work saturation levels of 75%, 100%, and 125% were analyzed for both powders. These settings automatically equate to different binder/powder volume ratios depending on the powder selected in the ZPrint software. The levels were selected such that the 125% saturation of the zp130 provided the same binder/powder ratio as the 75% level for the zp102.

Part position

Part accuracy may depend on the position of the part in the build chamber, although this effect may vary with machine type and actual condition. In this paper the parts were positioned to 9 different locations. The coordinates of the 9 specimens are depicted in Figure 4 and presented in Table 2. The origin used in this work is shown Figure 3.

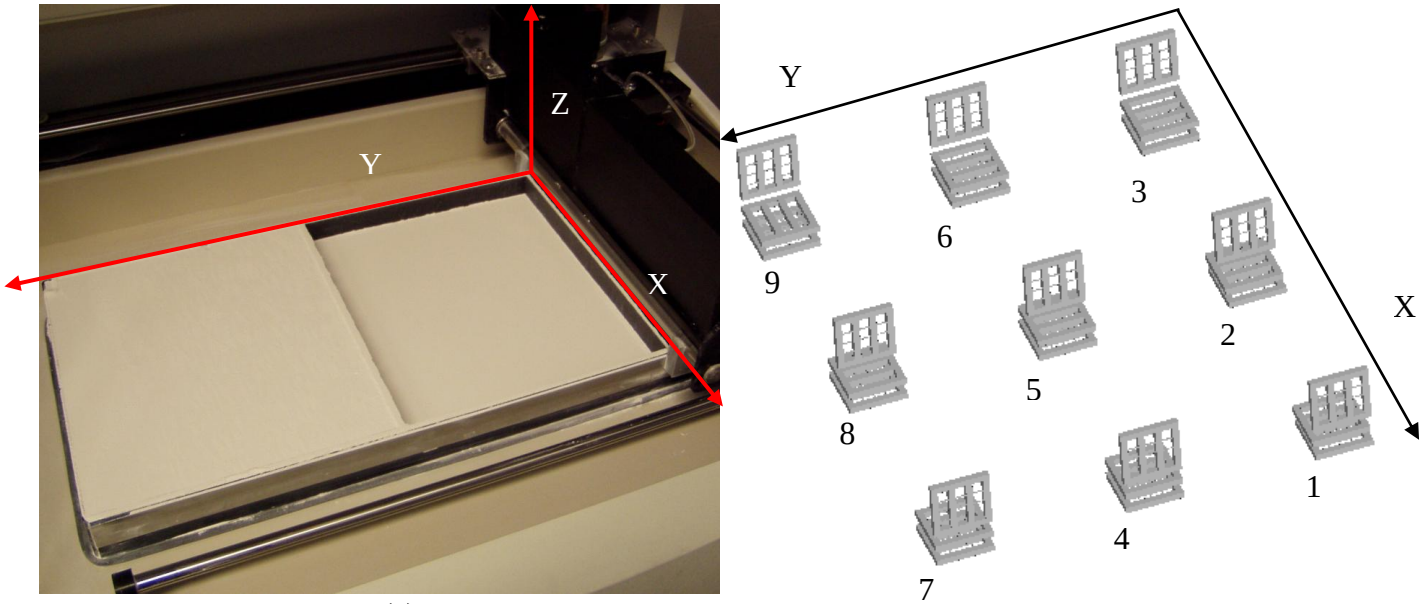

(a) (b)

Figure 3 (a) Picture of build chamber and co-ordinate system used and (b) indication of the locations of the specimens within the build chamber.

X axis / Y axis	Left (mm)		Center (mm)		Right (mm)	
	X	Y	X	Y	X	Y
Left (mm)	251	176	125.5	176	0	176
Center (mm)	251	88	125.5	88	0	88
Right (mm)	251	0	125.5	0	0	0

Table 2 Coordinates of the locations at which the parts were printed.

Orientation

Dimensional accuracy of the part is determined by the powder particle size in every direction but the accuracy in the x-y plane in more constrained by the hardware and control software. The resolution in the x (fast) and y (slow) axes depends on the printer head type (300 dpi) and the printing method. The actual size of the features in the z direction depends on their position along the z axis. If the feature size in the z direction is smaller than the layer thickness, the replicated size will either be the layer thickness or twice the layer thickness as the feature can be positioned within one or between two layers. This means printing a 0.4 mm thick feature with 0.0875mm layer thickness can result in five (5 x 0.875=4.375 mm) or six layers (6 x 0.875= 5.25 mm) according to its position along the z axis

The accuracy of the 3DP system in the x, y, and z directions was assessed by printing specimens with the examined dimensions in these directions as shown in Figure 5.

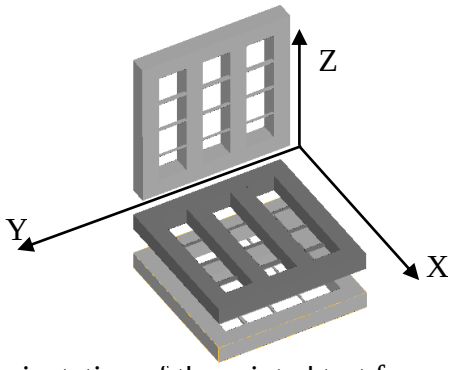

Figure 5 Schematic of the orientation of the printed test frames in location three, six and nine

Measuring Accuracy

The beams were measured using a Reichert MeF2 (Reichert, Vienna, Austria) inverted light optical microscope from one direction, that is the beams that were oriented in the x and y directions were measured in the x-y plane while the beams in the z direction were measured in the y-z plane. First, the captured images were thresholded and then the average chord length in the horizontal direction was calculated using the Buehler Omnimet image analysis software (Buehler Ltd. Lake Bluff, IL, USA). On each specimen the nine beams were measured separately, the average of the three measurements for beams of similar size was calculated and recorded. An accuracy value of comparison for the beams was calculated by dividing the measured values by the nominal dimensions. The results of the full factorial design were analyzed and evaluated with Design-Expert 7.0 design of experiments software (Stat-Ease Inc. Minneapolis, MN, USA).

Results and discussion

The results for the particle size distribution measurement of both powders are shown in Figure 6. There was no significant difference between the mean particle size diameters: it was 41.03µm for the zp102 and 40.79µm for the zp130. The distribution curves showed a noted difference between 2 and 10 µm with a reduced amount of particles present in the zp130 powder. The zp102 had fewer particles between 10 µm and 40 µm but more particles below 10µm. For the zp102 19.3% of the powder particles were between 1 and 10 µm and 32.6% were between 10 and 40 µm. For the zp130 powder these figures were 11.2% and 43.3% respectively.

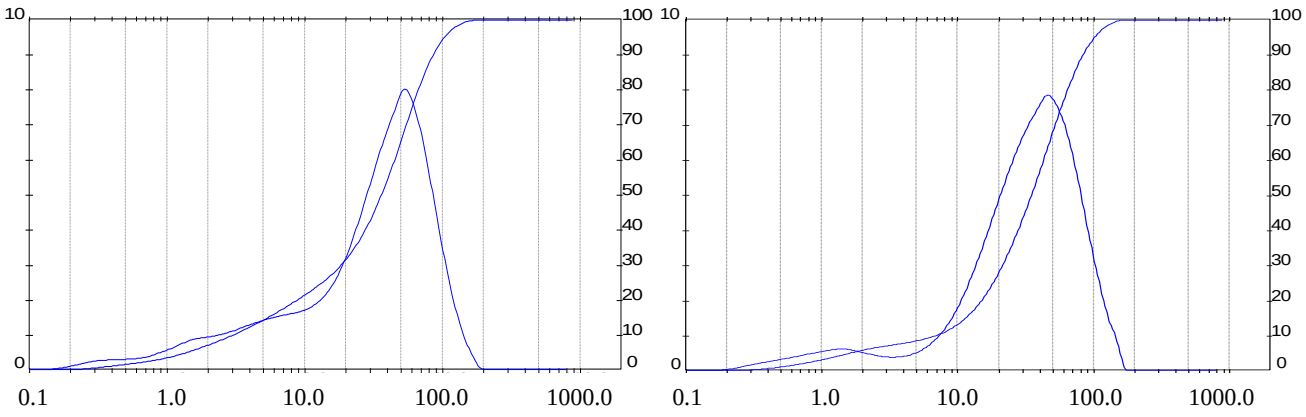

Figure 6 Particle size distributions for (a) zp102 and (b) zp130 powders with the x-axis in micrometers and the secondary y axis shown in percentage.

To find the factors that have a significant influence on the accuracy analysis of variance (ANOVA) was carried out. After eliminating the insignificant interactions the ANOVA results table for the two powders are presented separately in
Table **3** and Table 4.

Source	Sum of squares	Degrees of freedom	Mean square	F value	P value
Model	532362.57	12	44363.55	168.56	< 0.0001
A-Saturation	2.23	1	2.23	0.01	0.9268
B-Size	123249.45	1	123249.45	468.29	< 0.0001
C-Orientation	388540.24	2	194270.12	738.14	< 0.0001
D-X position	183.27	1	183.27	0.70	0.4049
E-Y position	2701.25	1	2701.25	10.26	0.0015
AB	1269.73	1	1269.73	4.82	0.0291
AD	1997.97	1	1997.97	7.59	0.0063
CD	6061.70	2	3030.85	11.52	< 0.0001
A^2	4589.95	1	4589.95	17.44	< 0.0001
B^2	3766.78	1	3766.78	14.31	0.0002
Residual	60533.63	230	263.19	-	-
Total	592896.20	242	-	-	-

Table 3 ANOVA table for zp102

Source	Sum of squares	Degrees of freedom	Mean square	F value	P value
Model	867823.29	18	48212.41	311.35	< 0.0001
A-Saturation	6606.40	1	6606.40	42.66	< 0.0001
B-Size	155766.06	1	155766.06	1005.91	< 0.0001
C-Orientation	666043.07	2	333021.54	2150.59	< 0.0001
D-X position	34.15	1	34.15	0.22	0.6391
E-Y position	471.62	1	471.62	3.05	0.0823
AB	1085.68	1	1085.68	7.01	0.0087
AC	11894.83	2	5947.42	38.41	< 0.0001
BC	7958.98	2	3979.49	25.70	< 0.0001
CD	1740.73	2	870.36	5.62	0.0042
CE	1915.44	2	957.72	6.18	0.0024
B^2	13058.95	1	13058.95	84.33	< 0.0001
D^2	540.03	1	540.03	3.49	0.0631
E^2	707.35	1	707.35	4.57	0.0337
Residual	34686.67	224	154.85	-	-
Total	902509.97	242	-	-	-

Table 4 ANOVA table for zp130

From the results it can be concluded that the F value was high for both models which means the model was significant and there was only a 0.01% chance that this occurred due to noise. The F values for the factors were calculated by dividing the means square of the factor by the residual mean square. Results with p values less than 0.05 indicate that they are significant factors. According to this, significant factors for zp102 are size, orientation, and y position and for zp130 saturation, size, and orientation are. Several other model terms, interactions are also concerned significant. The contribution of the most significant factors in is presented at Figure 7

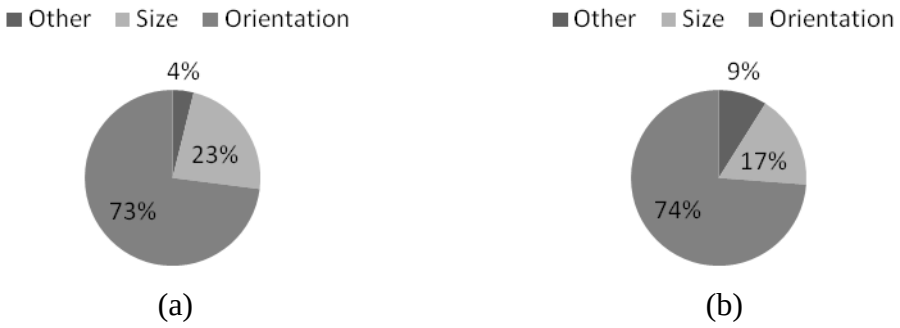

(a) (b)

Figure 7 Contribution of the factors in the model for (a) zp102 and (b) zp130

Figure 8 represents the effect of the beam size and the saturation on the normalized accuracy which is noted as the percentage of measured divided by nominal on the y-axis of these graphs. This represents the percentage increase of the prototype dimension over the dimension set in the CAD file. It can be concluded that increasing the size considerably increased the accuracy for both powders. There was little difference between the zp102 and zp130 powder for the 0.3 mm beam size (see Figure 8 (a) and 8 (b)). The accuracy was 20% higher with the zp130 powder compared to zp102 powder for the 0.5 mm beam. According to the results of ANOVA in Table 3

saturation factor was not significant for the zp102. Using the zp130 powder the higher saturation improved the accuracy although its influence was very small compared to beam size.

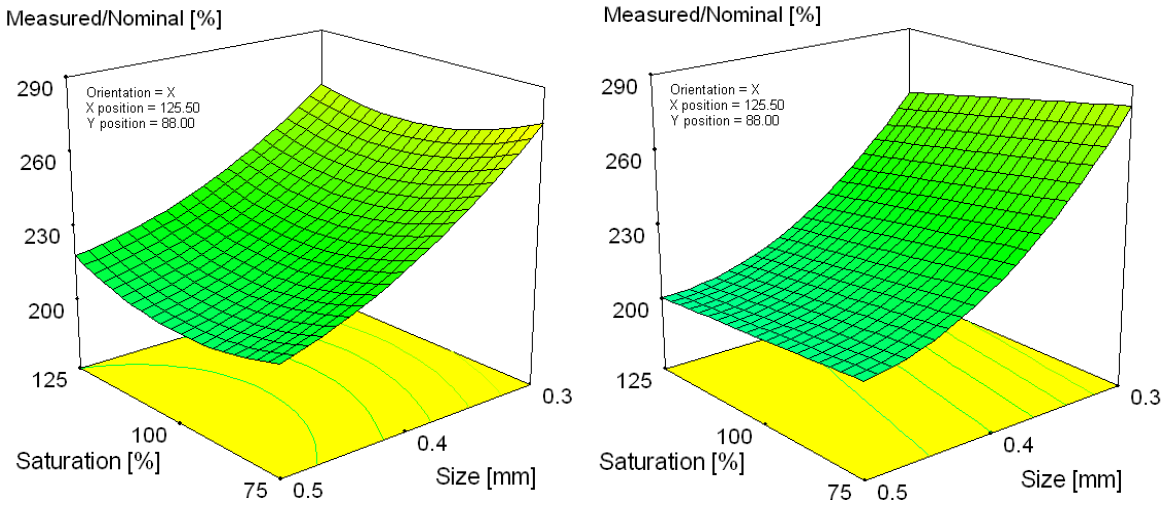

Figure 8 Size and saturation factor influence on accuracy for (a) zp102 and (b) zp130

The orientation had the most powerful influence in both powders and especially so for the zp130, see Figure 9 (a) and (b).

The results that are presented in Figure 9 indicate that there was no considerable difference in the x and y direction for the zp102 but there was 30% (measured/nominal) difference for the zp130. In the z direction the manufactured beam size was significantly lower and closer to the set size. However there was a very large difference between the x and y, and the z axis. This is probably due to the fact that manufacturing in the z direction is less sensitive to the printer head positioning which may be responsible for the higher inaccuracy in the x-y plane.

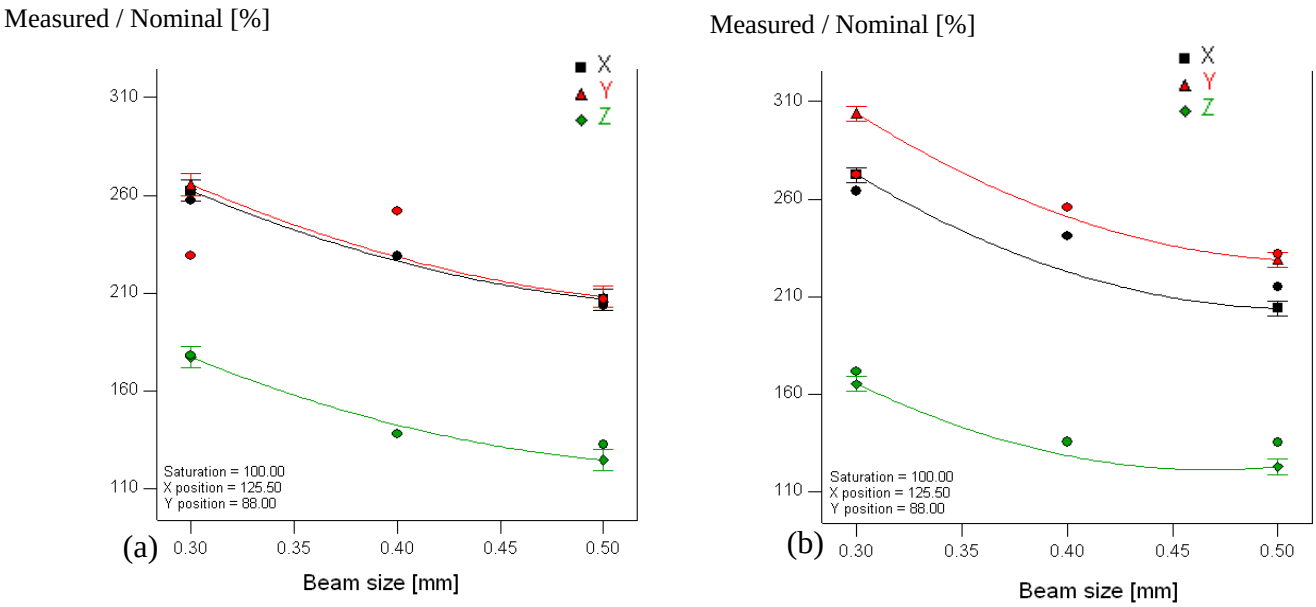

Figure 9 Percentage beam accuracy in relation to beam size and orientation at a saturation of 100% for (a) zp102 and (b) zp130

Figure 10 shows the actual sizes of the beams as measured with the Reichert microscope. Examining the actual average measured values for the sizes of 0.3 and 0.4 mm beams it can be established that there is no difference between the figures. The difference between the width of the 0.5 mm and the 0.3 - 0.4 mm beams was between 90 and 120 µm indicating that the machine used the same number of layers when it printed the 0.3 and 0.4 mm size beams and laid one extra layer to print the 0.5 mm beams. These results confirm that the accuracy of the beams in the z direction depends on their actual position along the z axis as described above.

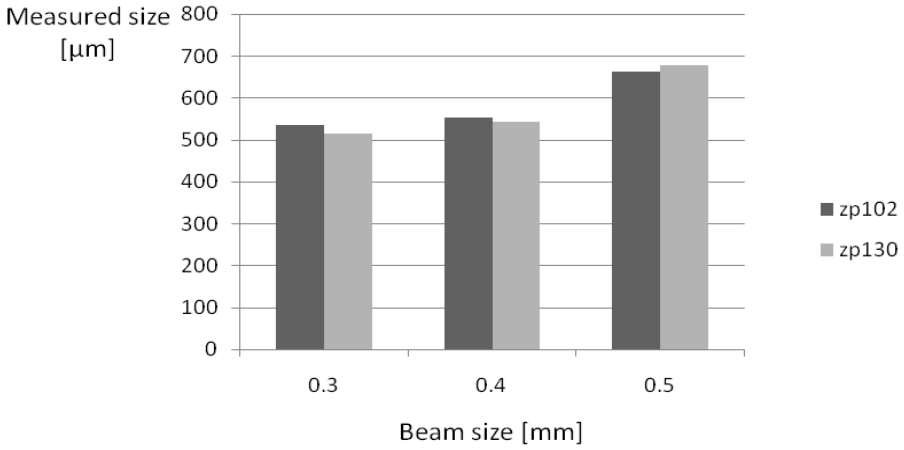

Figure 10 Actual measured beam sizes in the z direction at 100% saturation in position 5

Comparing the results for the two powders where the same binder/volume ratio was used (that is 75% for the zp102 and 125% for the zp130) no significant difference in accuracy was detected between the use of the two powders. The saturation settings parameter had very little influence on the accuracy in case of the zp102 powder (see Figure 9 (a) relative to Figure 11 (a)). The effect of saturation was however measurable for the zp130 (see Figure 9 (b) relative to Figure 11 (b).

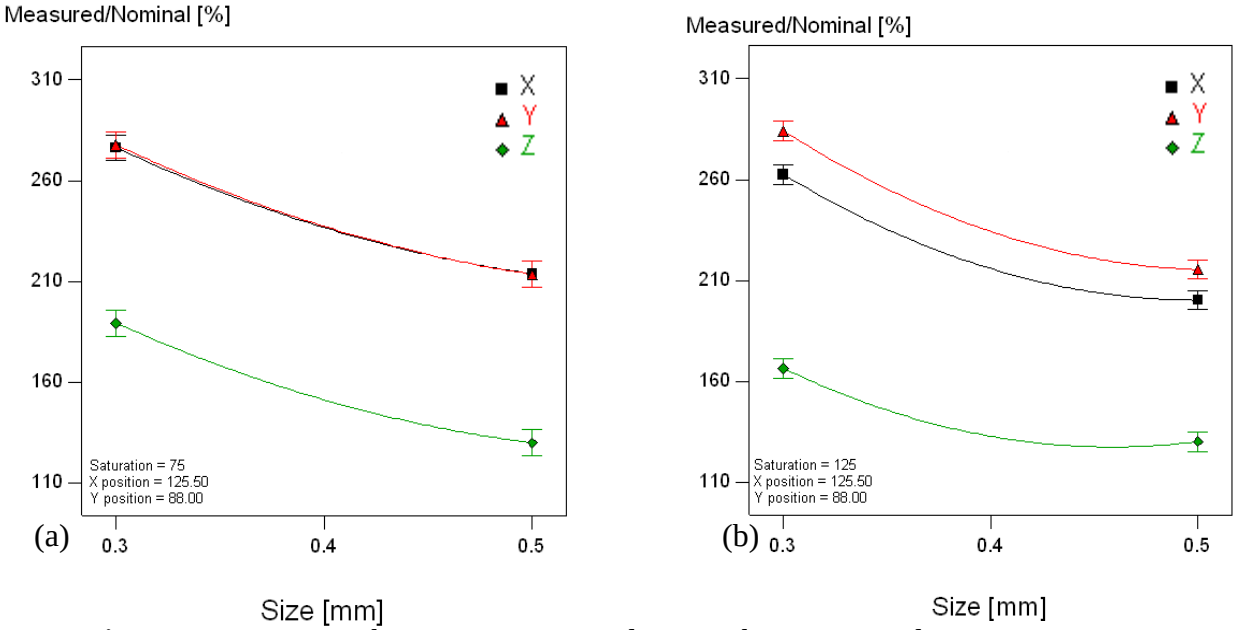

Figure 11 Percentage beam accuracy in relation to beam size and orientation at a saturation of 75% for (a) zp102 and at a saturation of 125% for (b) zp130

According to the ANOVA tables the x position is not a significant factor but the part position along the y axis may have some contribution in the final part accuracy. The accuracy maps of the 3D printer were drawn up from the results of the nine different locations, see Figure 12 and 13. The positions of best accuracy are indicated with "+" symbol and the locations that provided the least accurate beams are noted with "–" symbol. The results did not show significant differences; however with the zp102 powder the positions closer to the x axis did show better accuracy.

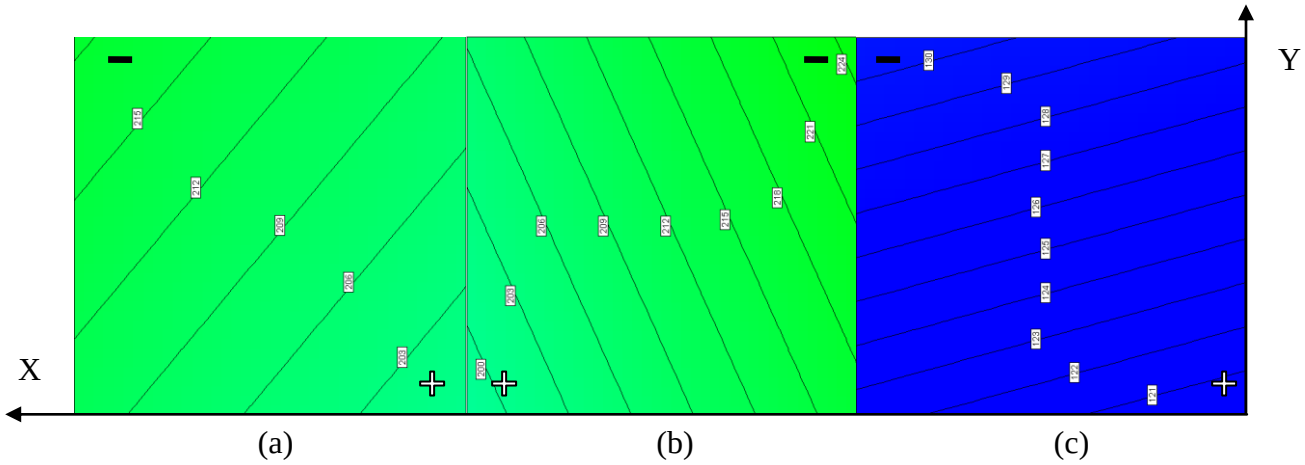

Figure 12 Accuracy map of the build chamber for zp102 in (a) x, (b) y, and (c) z orientations.

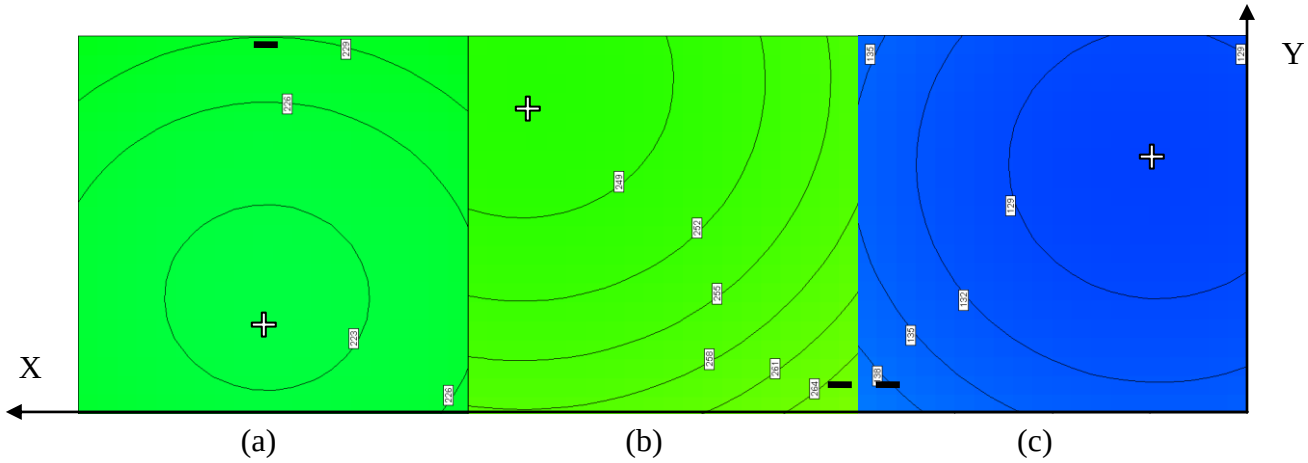

Figure 13 Accuracy map of the build chamber for zp130 in x (a), y (b), and z (c) orientations.

Conclusions and further directions

Saturation was not seen to have a significant effect for the zp102 powder but larger saturations were seen to increase the accuracy slightly for the zp130 powder. Changing the saturation showed very small influence on the accuracy but low shell saturation levels made the samples very fragile that rendered the specimen removal and depowdering difficult. Comparing the two powder types it can be concluded that there is no substantial difference in accuracy in the examined size range.

The sizes produced in the x and y direction were approximately 2.5 times their nominal dimensions and in the z direction were approximately 1.5 times their nominal dimensions. An

improvement in accuracy was noted for larger beam sizes. The measurements in the x and y orientations showed were similar for the zp102 but were better in the x-direction compared to the y-direction for the zp130. The closest recorded result to the 300 μm size was 464 μm which was obtained at 75% saturation, in the z-direction, and with the zp130 powder. The zp130 powder, in the z-direction and with saturation at 75% and 100% produced the smallest deviations from the actual beam set dimension. The lowest percentage deviation was noted for the 0.5 mm with the zp130 powder at about 30%. The zp130 powder produced a deviation on average 51 μm better than with the zp102 in the z-direction. The much better accuracy in the z-direction indicates that the positioning of the printer head in the x and y direction may be the main boundary in manufacturing small features.

Two important factors however affecting the accuracy at this scale are the number of printer head nozzles that are firing and the actual size of the powder layer brought across during the process. The printer head nozzles are arranged in a zigzag pattern with diameters of 60 μm with approximately 25 μm spacing between them. The firing of three of these nozzles would equate to a line of binder of approximately 255 μm and four to a line of 340 μm. The discrete nature of this process results in a compromised resolution in the y direction on levels examined in this work. The powder layer will also be variable to the extent that the powder with particle sizes ranging from 0 to 200 μm will lead to a variable layer height somewhere in between depending on packing density and pressure that may also contribute to the accuracy in the z direction. The position along the z axis may also influence the accuracy however this effect can be easily accounted for as described above. Not withstanding these complications binder bleeding also presents a considerable possibility for deterioration in dimensional tolerances which could justify the oversized beams noted in this work.

The printed 500 μm beam size is viable for scaffold geometries although the accuracy especially in the x-y plane is not acceptable for tissue engineering application. Part position in the build chamber changes the accuracy somewhat but significant trends could not be detected and its contribution in the results was negligible compared to the other factors. Further investigations will include various biocompatible powders including starch, and biodegradable polymers with appropriate binders using various particle sizes and particle size distributions. Sieving the powder is one way to make batches with different particle sizes although this process for large amounts is found to be inefficient. The effect of the saturation settings on mechanical properties will be further investigated in the future.

Acknowledgements

This research has been supported by a Marie Curie Early Stage Research Training Fellowship of the European Community's Sixth Framework Programme under contract number MEST-CT-2005-020621.

References

1. Hutmacher, D.W., Journal of Biomaterials,VSP, 2000, 21, pp. 2529-2543.
2. Sachlos, E., and Czernuszka, J.T., European Cells and Materials, European Cells & Materials Ltd, 2003, 5, pp. 29-40.
3. Bonzani, I.C., George, J.H., and Stevens, M.M., Current Opinion in Chemical Biology, Elsevier, 2006, 10, pp. 568–575.
4. Martina, M., and Hutmacher, D.W., Polymer International, Wiley InterScience 2007, 56, pp.145–157
5. Hutmacher, D.W., Journal of Biomaterials Science, Polymer Edition, VSP, 2004, 12, pp. 107-124.
   Lam, C.F., Mo, X.M., Teoh, S.H. Hutmacher, D.W.
6. Materials Science and Engineering, Elsevier, 2002, C 20, pp. 49-56.
7. Hutmacher, D.W., Sittinger, M. and Risbud, M.V., Trends in Biotechnology, Elsevier, 2004, 22, 7, pp. 354-361.
8. Botchwey, E.A., Dupree, M.A., Pollack ,S.R., Levine, E.M., and Laurencin, C.T., Journal of Biomedical Materials Research, Wiley Periodicals Inc., 2003, 67(1), pp. 357–67.
9. Hollister, S.J., Nature Materials, Nature Publishing Group 2005, 4, pp. 518-523.
10. Leukers, B., Journal of Materials and Medicine, 2005, 16, pp. 1121-1124.
11. Seitz, H., Rieder, W., Irsen, S., Leukers, B., Tille, C., Journal of Biomedical Materials Research, Part B: Applied Biomaterials, Wiley Periodicals Inc., 2005, 74B, pp. 782–788.
12. Szucs, T.D., Eosoly, S., Brabazon, D., and Olah, L., 8th National Conference on Rapid Design,
    Prototyping and Manufacture, Professional Engineering Publishing Ltd., 2007 pp. 3-11.
13. Yao, A.W. and Tseng, Y.C., Rapid Prototyping Journal, MCB UP Limited, 2002 Vol. 8, No. 3, pp. 180–189